nature photonics

LETTERS

PUBLISHED ONLINE: 11 MAY 2014 | DOI: 10.1038/NPHOTON.2014.83

Coherent phase-matched VUV generation by field-controlled bound states

Michael Chini[1], Xiaowei Wang[1,2], Yan Cheng[1], He Wang[3], Yi Wu[1], Eric Cunningham[1], Peng-Cheng Li[4,5], John Heslar[4], Dmitry A. Telnov[6], Shih-I Chu[4,7] and Zenghu Chang[1]*

The generation of high-order harmonics[1] and attosecond pulses[2] at ultrahigh repetition rates (>1 MHz) promises to revolutionize ultrafast spectroscopy. Such vacuum ultraviolet (VUV) and soft X-ray sources could potentially be driven directly by plasmonic enhancement of laser pulses from a femtosecond oscillator[3,4], but recent experiments suggest that the VUV signal is actually dominated by incoherent atomic line emission[5,6]. Here, we demonstrate a new regime of phase-matched below-threshold harmonic generation, for which the generation and phase matching is enabled only near resonance structures of the atomic target. The coherent VUV line emission exhibits low divergence and quadratic growth with increasing target density up to nearly 1,000 torr mm and can be controlled by the sub-cycle field of a few-cycle driving laser with an intensity of only $\sim 1 \times 10^{13}$ W cm^{-2}, which is achievable directly from few-cycle femtosecond oscillators with nanojoule energy[7].

High-order harmonic generation (HHG) has been the enabling technology for ultrafast science in the VUV and soft-X-ray spectral regions. Recently, ultrafast sources of below-threshold harmonics[1,3], with photon energies below the target ionization potential, have been demonstrated. Such harmonics are critical to the extension of time-resolved photoemission spectroscopy[8] to megahertz repetition rates and to the development of high-average-power VUV sources, because they can be generated with relatively low driving laser intensities ($\sim 1 \times 10^{13}$ W cm^{-2}). Ultrafast VUV sources of low-order harmonics are also critical tools for studying wave packet dynamics in bound states of atoms[9] and molecules[10]. However, compared to the high-order above-threshold harmonics, which have been extensively studied, little attention has been devoted to the development and characterization of below-threshold harmonic sources.

Although below-threshold harmonic generation is largely incompatible with the three-step model of HHG[11], recent experiments[1,12] indicate that below-threshold harmonics can arise from a non-perturbative process. This non-perturbative generation mechanism has been attributed to negative energy returns of electron trajectories initiated by over-the-barrier ionization and driven by the oscillating laser field[13]. However, such semi-classical treatment minimizes the influence of the target atom, an approach that may not be valid for below-threshold harmonics, where resonance enhancement has been observed for moderate driving laser intensities[14]. Here, we uncover a novel regime of below-threshold harmonic generation accompanied by bright, coherent VUV line emission. The coherent VUV source results from the interaction of moderately intense few-cycle driving laser pulses with atomic targets, wherein below-threshold harmonics are enhanced near atomic resonances. In contrast to the incoherent plasma line emission observed in HHG with high laser intensities or with plasmonic enhancement[5,6], the resonance-enhanced VUV emission is spatially coherent, with high conversion efficiency and phase-matched growth. We further find that the VUV emission exhibits non-perturbative behaviour and can be controlled by the field of the driving laser. Because the VUV source requires few-cycle driving lasers with an intensity of only $\sim 1 \times 10^{13}$ W cm^{-2}, it is readily extendable to ultrahigh repetition rates with commercially available Ti:sapphire oscillators[7].

In the experiment, below-threshold harmonics were generated from argon and the angularly resolved VUV spectrum was measured using a flat-field grating spectrometer[15]. The harmonic generation was driven with few-cycle (~5 fs) near-infrared (~730 nm) laser pulses, loosely focused to moderate intensities ($\sim 1 \times 10^{13}$ to 1×10^{14} W cm^{-2}) sufficient to generate harmonics around the ionization threshold, but not so high as to destroy the atomic resonances[16]. The use of few-cycle driving lasers results in spectrally broad harmonics, and multiple resonances can be observed within a single harmonic.

Figure 1a shows the spectrally and angularly resolved VUV signal in the vicinity of the 9th and 11th harmonics with a driving laser intensity of $(3.3 \pm 0.3) \times 10^{13}$ W cm^{-2} and a target pressure–length product of 10 torr mm. Whereas the 11th harmonic is above the argon ionization threshold ($I_p = 15.76$ eV), the 9th harmonic spans photon energies both above and below threshold. Below threshold, the 9th harmonic exhibits narrow-linewidth spectral enhancements in the vicinity of the atomic resonances. Figure 1b shows the evolution of these resonance-enhanced structures (RESs) as a function of the driving laser intensity within three different regimes. At relatively low intensities ($\sim 1 \times 10^{13}$ W cm^{-2} to 3×10^{13} W cm^{-2}), the RESs exhibit narrow linewidths and dominate the harmonic spectrum. For intensities between $\sim 3 \times 10^{13}$ W cm^{-2} and 8×10^{13} W cm^{-2}, the above-threshold harmonic emission becomes comparable to the RESs and the lines in general become shifted and broadened until no resonances can be observed at intensities higher than $\sim 1 \times 10^{14}$ W cm^{-2}. The positions of the RESs agree qualitatively with the resonance energies of argon, and the resonance enhancement is further confirmed by below-threshold harmonic generation in neon and xenon gases, and by numerical solution of the time-dependent Schrödinger equation (see Supplementary Section 'Simulated harmonic spectra').

[1]Institute for the Frontier of Attosecond Science and Technology, CREOL and Department of Physics, University of Central Florida, Orlando, Florida 32816, USA, [2]Department of Physics, National University of Defense Technology, Changsha, Hunan 41000, China, [3]Materials Sciences Division, Lawrence Berkeley National Laboratory, Berkeley, California 94720, USA, [4]Center for Quantum Science and Engineering and Department of Physics, National Taiwan University, Taipei 10617, Taiwan, [5]College of Physics and Electronic Engineering, Northwest Normal University, Lanzhou, Gansu 199034, China, [6]Department of Physics, St Petersburg State University, St Petersburg 199034, Russia, [7]Department of Chemistry, University of Kansas, Lawrence, Kansas 66045, USA.
*e-mail: zenghu.chang@ucf.edu

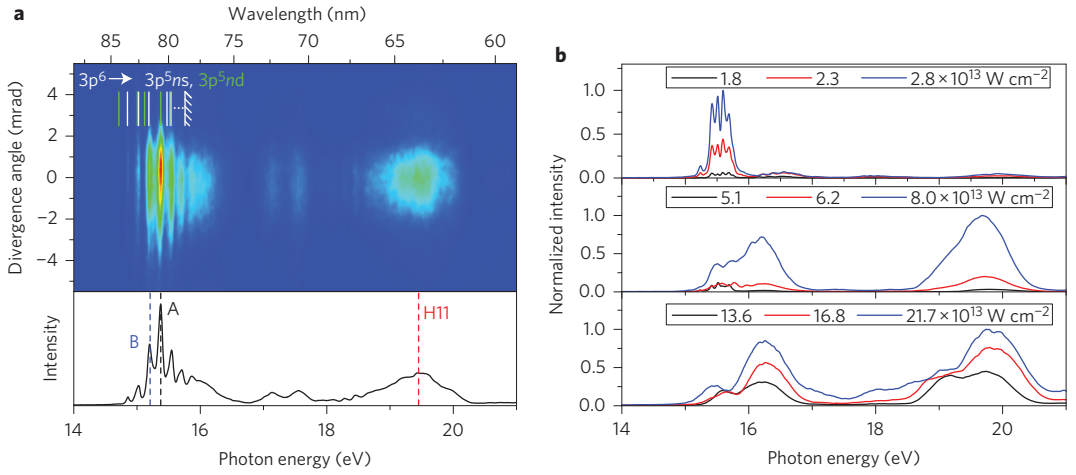

Figure 1 | Resonance-enhanced structures in below-threshold harmonic generation. a, Measured harmonic spectrum with an intensity of $(3.3 \pm 0.3) \times 10^{13}$ W cm^{-2} and a target pressure–length product of 10 torr mm. The spectrum is characterized by coherent line emissions (for example, RESs A and B) which lie within the energy range of the labelled $3p^6 \rightarrow 3p^5ns$ (white vertical lines) and $3p^5nd$ (green vertical lines) resonance manifolds of argon in addition to the relatively broad high harmonics (for example, the 11th harmonic, H11). **b**, Evolution of the resonance-enhanced structures with driving laser intensity. At low intensities (top), the resonance-enhanced structures dominate the spectrum, whereas the harmonics dominate at higher intensities (bottom).

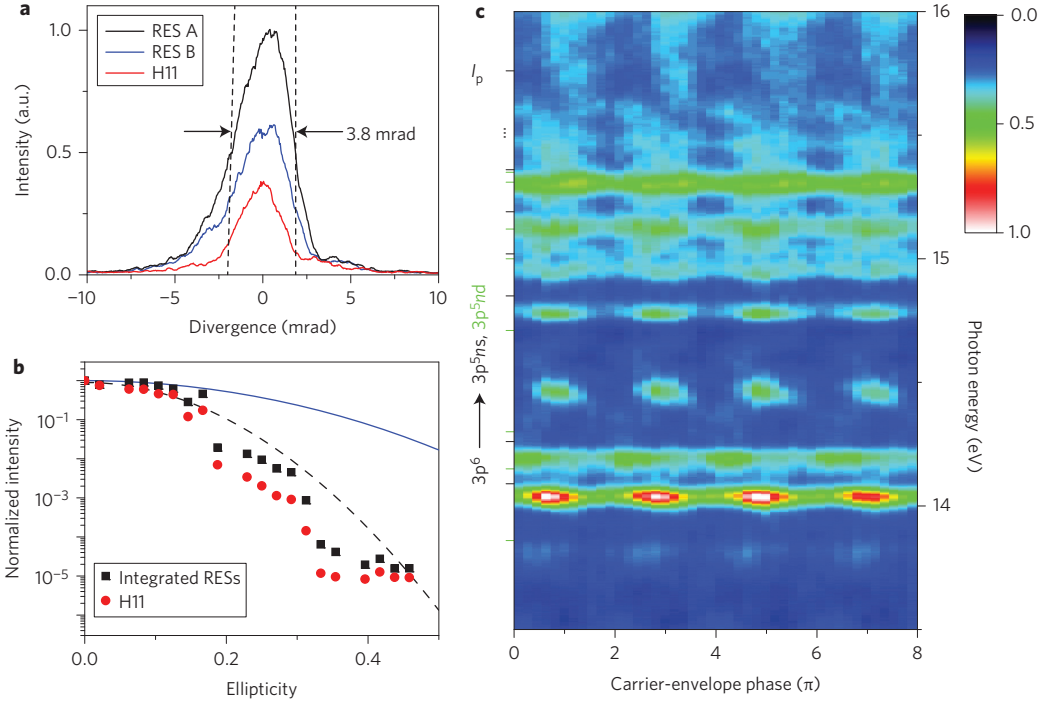

Figure 2 | Strong-field control of resonance-enhanced structures. a, Both the RESs (A and B) and the above-threshold harmonics exhibit narrow divergence angles of <4 mrad full-width at half-maximum, indicating laser-like spatial coherence of the VUV line emission. **b**, The efficiency of the coherent line emission depends strongly on the ellipticity of the driving laser. The measured ellipticity dependence is much stronger than that predicted for perturbative generation of the 9th harmonic (blue solid line), but agrees qualitatively with the extrapolated ellipticity dependence of the 9th harmonic from ref. 17 (black dashed line). **c**, The RESs exhibit a strong dependence on the carrier-envelope phase when the VUV generation is confined to a single half-cycle of the driving laser.

Although spectrally similar to atomic line emission, the observed RESs are emitted in a laser-like beam, with divergence angles similar to the above-threshold harmonics, as shown in Fig. 2a. Such a small divergence (<4 mrad) is consistent with previous measurements of below-threshold harmonics in a tight focusing geometry, wherein multiple divergence angles were attributed to quantum trajectories ('short' and 'long') with different intensity-dependent phases[1]. Here, the phase-matching conditions favour the on-axis harmonic emission, and the more strongly divergent long trajectory contributions are not observed. Although previous studies have indicated that the on-axis short trajectory contributions cannot be explained using classical trajectories initiated by tunnel ionization[13], we observe signatures of non-perturbative behaviour and field control in the generation of RESs. In Fig. 2b, the integrated yield of the RESs between 15 and 15.8 eV is compared to that of the above-threshold 11th harmonic for elliptically polarized driving pulses with the same intensity as in Fig. 1a. The dependence of the VUV intensity on the driving laser ellipticity is much stronger

than that predicted by perturbative harmonic generation for both the RESs and the 11th harmonic, as the efficiency is reduced by an order of magnitude when the ellipticity is ~0.2. Such strong ellipticity dependence is in good agreement with previous measurements of above- and below-threshold harmonics[17,18] with more intense few-cycle lasers, and suggests the possibility of temporally 'gating' the RES generation by shaping the driving laser polarization. Figure 2c shows the dependence of VUV generation on the carrier-envelope phase of the driving laser using the double optical gating technique[19], which produces an effective sub-cycle gate with linear polarization. The observed modulation of the RES yield with a 2π periodicity is consistent with the double optical gating and indicates field control of the RES emission. The effects of the carrier-envelope phase on the intensity of the RES are much stronger than that observed with linearly polarized 5 fs pulses (see Supplementary Section 'Carrier-envelope phase dependence').

Generation of bright VUV sources requires that careful attention be paid to the phase-matching of the harmonic light and the laser-driven polarization, allowing coherent build-up of the harmonic field in the macroscopic medium. For above-threshold HHG, phase-matching is achieved by balancing the change of the driving laser phase associated with the plasma density variation, the neutral atom dispersion, the Gouy phase shift and the intensity-dependent atomic dipole phase[20]. Perfect phase-matching characterized by quadratic growth of the high-order harmonic yield with gas pressure can be achieved in optimized cases and the phase-matched photon flux is limited only by absorption[21]. On the other hand, phase-matching of the below-threshold harmonics is not limited by absorption. In Fig. 3a, the phase-matched yield of the RESs between 15 and 15.8 eV is compared with that of the 11th harmonic under the same intensity as in Fig. 1a. While the phase-matching of the 11th harmonic is limited by reabsorption of the harmonic photons by the generating gas to pressure–length products of ~20 torr mm, we find that the below-threshold RESs can be perfectly phase-matched to much higher pressures—up to nearly 1,000 torr mm—allowing a relative enhancement of approximately four orders of magnitude over the 11th harmonic. With a pressure–length product of 10 torr mm (36 torr mm), we find the total energy in the RESs to be 0.35 ± 0.1 nJ (4.0 ± 0.5 nJ) at the generation target, giving an energy conversion efficiency of 3.5×10^{-6} (4.0×10^{-5}). At the highest phase-matched pressure, the quadratic scaling yields an efficiency greater than 1% and an extrapolated flux of more than 1 μJ. Numerical simulations (see Supplementary Section 'Macroscopic propagation'), shown in Fig. 3b, indicate that the phase-matching occurs primarily in the vicinity of the resonances, in agreement with the experiment.

In the vicinity of the resonance manifold, the total phase-mismatch Δk between the harmonic field and the laser-driven polarization arises primarily from the phase-mismatch of the neutral atomic medium[22,23]

$$\Delta k_{\mathrm{at}}(\omega) \approx 2\pi N r_{\mathrm{e}} c\omega \sum_j \frac{f_j}{\omega_j^2 - \omega^2} \quad (1)$$

and of the Gouy phase

$$\Delta k_{\mathrm{G}}(z) \approx q \frac{1}{2\pi} \frac{\mathrm{d}}{\mathrm{d}z} \tan^{-1}\left(\frac{z}{z_{\mathrm{R}}}\right) \quad (2)$$

Here, z is the on-axis target position relative to the focal point, z_{R} is the Rayleigh range, q is the harmonic order, r_{e} is the classical electron radius, N is the atomic density, and ω_j and f_j are respectively the energy and oscillator strength of the jth resonance. For photon energies $\omega > \omega_j$, the resonance contribution to Δk_{at} is negative and can compensate the positive Gouy phase-mismatch, giving

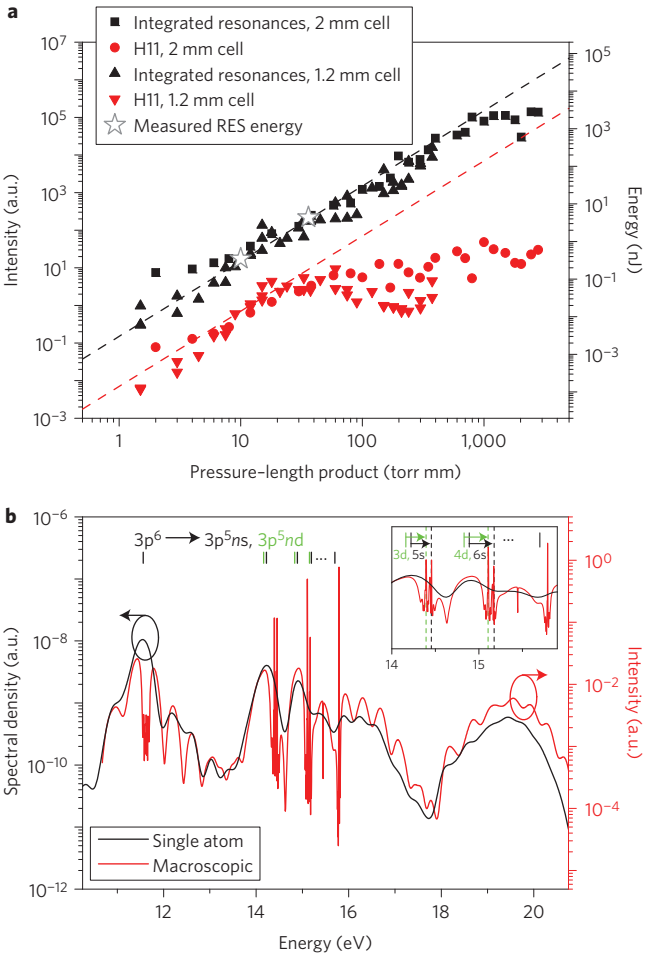

Figure 3 | Phase-matching of resonance-enhanced structures. a, The coherent VUV emission in the vicinity of the RESs scales quadratically with the target gas pressure–length product, indicating perfect phase-matching. The 11th harmonic (H11) scales quadratically up to a pressure–length product of only ~20 torr mm due to the strong absorption cross-section of the neutral gas for photon energies just above the ionization threshold. Calibrated energy measurements of the RESs are indicated by open grey stars, with the dashed lines indicating quadratic scaling serving to guide the eye. **b**, Numerical simulation of the VUV emission in argon indicates that the phase-matching process results in spectrally narrow, energy-shifted RESs when compared with single-atom emission. An enlarged view of the spectrum in the vicinity of the ionization threshold (inset) shows the shift in the phase-matched RES energy relative to the single-atom emission, which exhibits broad peaks located at the bound state resonance energies.

$\Delta k = \Delta k_{\mathrm{at}} + \Delta k_{\mathrm{G}} \approx 0$ under the experimental conditions, as shown in Fig. 4a. Because Δk_{at} is proportional to the atomic density, different photon energies are phase-matched at different target pressures. For our broadband source, covering multiple resonances, this leads to an energy shift of the RESs with increasing pressure. Figure 4b shows the pressure-dependent spectrum of the phase-matched emission. The clear energy shifts of the RESs indicate the resonance-assisted phase matching.

High-order harmonics generated at megahertz repetition rates are highly desirable for applications to ultrafast photoemission spectroscopy[24] and coincidence measurements, and can provide tabletop sources of high-average-power VUV light for lensless imaging[25] and nanoscale lithography. Here, we demonstrate a novel regime of phase-matched below-threshold harmonics, characterized by narrow-linewidth emission structures with a high conversion efficiency, potentially scalable to more than 1% of the driving laser

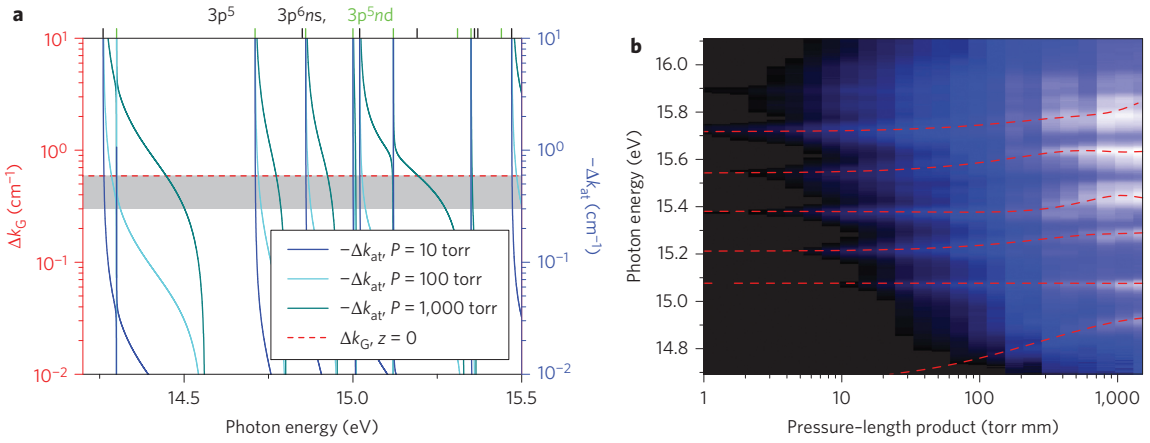

Figure 4 | Resonance-assisted phase-matching. a, Argon exhibits regions of pressure-dependent negative atomic phase-mismatch (solid lines) just above the atomic resonance energies, which can compensate the Gouy phase-mismatch (red dashed line) within the Rayleigh range (grey shading). **b**, Because the amount of negative atomic phase-mismatch increases with pressure, the phase-matched photon energy moves away from the resonance energy and the RESs tend to shift to higher energy with increasing pressure. The dashed red lines represent a cubic spline fit of the most prominent RES peak energies.

energy, which can be controlled by the sub-cycle field of the driving laser. Although there is still much to be learned regarding the generation of these RESs, the source holds substantial promise for advancing VUV spectroscopy to megahertz repetition rates. The required driving laser intensity of $\sim 1 \times 10^{13}$ W cm^{-2} is already achievable from few-cycle laser oscillators at the nanojoule level[7], opening the door to the development of compact, high-flux VUV light sources without the need for cavity or nanoplasmonic enhancement.

Methods

Experimental set-up. In the experiments, few-cycle (~5 fs) pulses from a Ti:sapphire amplifier with a hollow-core fibre and chirped mirror pulse compressor were loosely focused using a spherical mirror (f = 500 mm) to a gas cell (inner diameter = 1.2 mm, except where indicated) filled with argon gas. The cell was located ~6 mm after the focus, where on-axis harmonic generation was maximized. The focal spot beam waist was ~75 μm at the cell location, and the pulse energy was varied between ~5 and 300 μJ, corresponding to an intensity range of $\sim 1 \times 10^{13}$ to 6×10^{14} W cm^{-2}.

The spectrum of the high-order harmonics was then dispersed using a flat-field grating spectrometer[15] with a spectral resolution of ~40 meV at 15 eV. The grazing-incidence spherical grating focused the VUV light only along the dispersion direction, allowing simultaneous measurement of the spectrum and divergence of the high-order harmonics.

The absolute energy of the integrated RESs was measured using an XUV diode (IRD AXUV-100) after transmission through a 300 nm indium foil filter to block the fundamental driving laser and select the spectrum near 15 eV. Here, the driving laser intensity was slightly higher ($\sim 6 \times 10^{13}$ W cm^{-2}) to allow clear detection of the VUV signal level over the background level of the near-infrared laser only. The energies and conversion efficiencies represent the contribution of the RESs within the 9th harmonic only. The energy ratio of the RESs relative to the non-resonant 7th and 11th harmonics was determined by measuring the transmitted spectrum, and the transmission of the foil filter in the vicinity of the RESs was determined to be ~10%. The flux measurement was limited to small pressure–length products, because the indium foil was broken when the pressure exceeded 30 torr in the 1.2 mm generation cell. With a pressure–length product of 36 torr mm, the energy within the RES spectral region was measured to be 4.0 ± 0.5 nJ.

Ellipticity dependence. Elliptically polarized few-cycle pulses were produced by placing a zero-order half- and quarter-wave plate before the hollow-core fibre pulse compressor[26]. The major axis of the ellipse was kept constant to minimize the effects of the grating efficiency, which depends on the polarization of the VUV light. The degree of ellipticity and the major axis of the ellipse were measured just before the HHG set-up using a polarizer. For an ellipticity greater than 0.4, we found that the polarization was not well maintained through the chirped mirror compressor, and so the data with large ellipticities were discarded. For the perturbative harmonic generation shown in Fig. 2b, the harmonic yield is proportional to $[(1-\varepsilon^2)/(1+\varepsilon^2)]^{q-1}$, where ε is the ellipticity[27].

Simulated harmonic spectra. The simulated harmonic spectra were obtained by solving the time-dependent Kohn–Sham equations for the atom in the field using time-dependent density functional theory with a proper long-range exchange-correlation potential for argon[28–30] and by propagating the driving laser field and the generated harmonic field through the macroscopic medium according to the Maxwell wave equation[20]. The refractive index of the medium in the vicinity of the atomic resonances was calculated according to ref. 23, using the atomic energy levels obtained from the argon potential. The driving laser field consisted of a ~5 fs full-width at half-maximum sine-squared pulse with a central wavelength of 730 nm sitting upon a weak (4% peak intensity) pedestal with ~24 fs pulse duration. Except where noted otherwise, the gas target had a length of 2 mm with a constant pressure of 10 torr. The cell was positioned 2 mm after the focal spot with a beam waist of 35 μm. Detailed discussion of the calculations can be found in the Supplementary Sections 'Simulated harmonic spectra' and 'Macroscopic propagation'.

Received 2 August 2013; accepted 20 March 2014; published online 11 May 2014

References

1. Yost, D. C. *et al.* Vacuum-ultraviolet frequency combs from below-threshold harmonics. *Nature Phys.* **5,** 815–820 (2009).
2. Krebs, M. *et al.* Towards isolated attosecond pulses at megahertz repetition rates. *Nature Photon.* **7,** 555–559 (2013).
3. Kim, S. *et al.* High-harmonic generation by resonant plasmon field enhancement. *Nature* **453,** 757–760 (2008).
4. Park, I.-Y. *et al.* Plasmonic generation of ultrashort extreme-ultraviolet light pulses. *Nature Photon.* **5,** 677–681 (2011).
5. Sivis, M., Duwe, M., Abel, B. & Ropers, C. Extreme-ultraviolet light generation in plasmonic nanostructures. *Nature Phys.* **9,** 304–309 (2013).
6. Sivis, M. & Ropers, C. Generation and bistability of a waveguide nanoplasma observed by enhanced extreme-ultraviolet fluorescence. *Phys. Rev. Lett.* **111,** 085001 (2013).
7. Miranda, M. N., Oliveira, P. B., Bernardo, L. M., Kartner, F. X. & Crespo, H. M. Space–time focusing of phase-stabilized nanojoule-level 2.5-cycle pulses to peak intensities >3×10^{13} W/cm^2 at 80 MHz. *CLEO Europe* http://dx.doi.org/10.1109/CLEOE-EQEC.2009.5196426 (2009).
8. Rohwer, T. *et al.* Collapse of long-range charge order tracked by time-resolved photoemission at high momenta. *Nature* **471,** 490–493 (2011).
9. Chini, M. *et al.* Sub-cycle oscillations in virtual states brought to light. *Sci. Rep.* **3,** 1105 (2013).
10. Tao, H. *et al.* Ultrafast internal conversion in ethylene. I. The excited state lifetime. *J. Chem. Phys.* **134,** 244306 (2011).
11. Corkum, P. B. Plasma perspective on strong field multiphoton ionization. *Phys. Rev. Lett.* **71,** 1994–1997 (1993).
12. Power, E. P. *et al.* XFROG phase measurement of threshold harmonics in a Keldysh-scaled system. *Nature Photon.* **4,** 352–356 (2010).
13. Hostetter, J. A., Tate, J. L., Schafer, K. J. & Gaarde, M. B. Semiclassical approaches to below-threshold harmonics. *Phys. Rev. A* **82,** 023401 (2010).
14. Toma, E. S., Antoine, Ph., de Bohan, A. & Muller, H. G. Resonance-enhanced high-harmonic generation. *J. Phys. B* **32,** 5843–5852 (1999).
15. Wang, X., Chini, M., Cheng, Y., Wu, Y. & Chang, Z. *In situ* calibration of an extreme ultraviolet spectrometer for attosecond transient absorption experiments. *Appl. Opt.* **52,** 323–329 (2013).
16. Mevel, E. *et al.* Atoms in strong optical fields: evolution from multiphoton to tunnel ionization. *Phys. Rev. Lett.* **70,** 406–409 (1993).

17. Sola, I. J. *et al*. Controlling attosecond electron dynamics by phase-stabilized polarization gating. *Nature Phys.* **2,** 319–322 (2006).
18. Burnett, N. H., Kan, C. & Corkum, P. B. Ellipticity and polarization effects in harmonic generation in ionizing neon. *Phys. Rev. A* **51,** R3418 (1995).
19. Mashiko, H. *et al*. Double optical gating of high-order harmonic generation with carrier-envelope phase stabilized lasers. *Phys. Rev. Lett.* **100,** 103906 (2008).
20. Gaarde, M. B., Tate, J. L. & Schafer, K. J. Macroscopic aspects of attosecond pulse generation. *J. Phys. B* **41,** 132001 (2008).
21. Constant, E. *et al*. Optimizing high harmonic generation in absorbing gases: model and experiment. *Phys. Rev. Lett.* **82,** 1668–1671 (1999).
22. Kung, A. H., Young, J. F. & Harris, S. E. Generation of 1182-Å radiation in phase-matched mixtures of inert gases. *Appl. Phys. Lett.* **22,** 301–302 (1973).
23. Mahon, R., McIlrath, T. J., Myerscough, V. P. & Koopman, D. W. Third-harmonic generation in argon, krypton, and xenon: bandwidth limitations in the vicinity of Lyman-α. *IEEE J. Quantum Electron.* **15,** 444–451 (1979).
24. Hellmann, S., Rossnagel, K., Marczynski-Bühlow, M. & Kipp, L. Vacuum space–charge effects in solid-state photoemission. *Phys. Rev. B* **79,** 035402 (2009).
25. Sandberg, R. L. *et al*. Lensless diffractive imaging using tabletop coherent high-harmonic soft-X-ray beams. *Phys. Rev. Lett.* **99,** 098103 (2007).
26. Khan, S. D. *et al*. Ellipticity dependence of 400 nm-driven high harmonic generation. *Appl. Phys. Lett.* **99,** 161106 (2011).
27. Budil, K. S., Saliéres, P., L'Huillier, A., Ditmire, T. & Perry, M. D. Influence of ellipticity on harmonic generation. *Phys. Rev. A* **48,** R3437 (1993).
28. Tong, X.-M. & Chu, S.-I. Time-dependent density-functional theory for strong-field multiphoton processes: application to the study of the role of dynamical electron correlation in multiple high-order harmonic generation. *Phys. Rev. A* **57,** 452–461 (1998).
29. Telnov, D. A., Sosnova, K. E., Rozenbaum, E. & Chu, S.-I. Exterior complex scaling method in time-dependent density-functional theory: multiphoton ionization and high-order harmonic generation of Ar atoms. *Phys. Rev. A* **87,** 053406 (2013).
30. Chu, S.-I. Recent development of self-interaction-free time-dependent density-functional theory for nonperturbative treatment of atomic and molecular multiphoton processes in intense laser fields. *J. Chem. Phys.* **123,** 062207 (2005).

Acknowledgements

This work was funded by the Defense Advanced Research Projects Agency (DARPA) program in ultrafast laser science and engineering (PULSE) programme through a grant from Aviation and Missile Research, Development, and Engineering Center (AMRDEC), by the US Army Research Office (grant no. W911 NF-12-1-0456), and by the National Science Foundation (grant no. 106860). D.A.T. and S.-I.C. were partially supported by the US Department of Energy. P.-C.L., J.H. and S.-I.C. would also like to acknowledge the partial support of the National Science Council of Taiwan and National Taiwan University (grants nos 103R104021 and 103R8700-2).

Author contributions

M.C. and Z.C. conceived the study. M.C., X.W. and Y.C. designed the apparatus, performed the experiments and analysed the data. Y.W. and E.C. contributed to the carrier-envelope phase-dependent measurements and absolute energy calibration. M.C., H.W. and Z.C. developed the phase-matching model and interpreted the results. J.H. and D.A.T. performed the single-atom time-dependent Schrödinger equation calculations, while P.-C.L. performed the macroscopic calculations. The theoretical effort was coordinated by S.-I.C. All authors contributed to writing and editing the manuscript.

Additional information

Supplementary information is available in the online version of the paper. Reprints and permissions information is available online at www.nature.com/reprints. Correspondence and requests for materials should be addressed to Z.C.

Competing financial interests

The authors declare no competing financial interests.